CDF/PUB/EXOTIC/PUBLIC/10485

Search for a Standard Model Higgs Boson Decaying Into Photons at CDF Using 7.0 fb^{-1} of Data

The CDF Collaboration
URL http://www-cdf.fnal.gov
(Dated: April 18, 2011)

A search for the SM Higgs boson in the diphoton decay channel is reported using 7.0 fb^{-1} of data. The previous result used central photons ($|\eta| < 1.1$) collected from standard CDF photon selection. Here, we improve this identification by incorporating a new photon selection that uses a neural network to reject jet backgrounds. Sensitivity is also greatly improved by the addition of forward ($1.2< |\eta| < 2.8$) photons and the development of a new algorithm which selects photons that have converted into an electron-positron pair. 95% C.L. upper limits are set on the production cross section times the $H \to \gamma\gamma$ branching ratio for potential Higgs masses between 100 and 150 GeV/c^2.

Preliminary Results

I. INTRODUCTION

Low mass Higgs boson searches at the Tevatron usually focus on the dominant $b\bar{b}$ decay channel. The diphoton final state is appealing because the photon ID efficiency and energy resolution are much better than that of b-jets. The photon's better energy resolution leads to a narrow $M_{\gamma\gamma}$ mass peak which can be exploited to reduce backgrounds. In the standard model (SM), however, the branching fraction for the diphoton ($\gamma\gamma$) final state $B(H \to \gamma\gamma)$ has a maximal value of approximately 0.2% for Higgs masses of about 120 GeV/c^2. Nevertheless, we pursue this channel, not only because it is interesting to make a statement on the sensitivity of CDF to the standard model $H \to \gamma\gamma$ process, but also in order to contribute sensitivity to CDF's combined Higgs search along with the overall Tevatron Higgs search.

In addition to SM $H \to \gamma\gamma$ production, one can devise many possible Beyond the Standard Model (BSM) scenarios where $B(h \to \gamma\gamma)$ is enhanced. An informative summary of the various models that modify $B(h \to \gamma\gamma)$ can be found in Reference [1]. The "fermiophobic" Higgs (h_f) benchmark model assumes SM coupling to bosons and vanishing couplings to all fermions. The higher branching fraction causes a larger number of potential fermiophobic Higgs events compared to that predicted by the SM. Any resonance observed could also then be evidence for a BSM Higgs.

In the past, there have been phenomenological discussions of searches for h_f at the Tevatron experiments [2], as well as experimental searches at LEP [3]. In Run I, CDF searched for the fermiophobic Higgs [4] and recently for Run II, DØ published a paper [5] focusing on the same search. Most recently, CDF published a search for h_f with $\sim$3 fb^{-1} [6] and DØ published a search for the SM Higgs with $\sim$3 fb^{-1} [7].

Here, we will focus on the sensitivity of a CDF search for SM $H \to \gamma\gamma$. The first SM result in this channel by CDF was obtained using 5.4 fb^{-1} of data with "central" photons (η <1.1), giving a 95% C.L. expected upper limit of 19.4 on $\sigma \times B(h \to \gamma\gamma)$/SM [8] at a Higgs mass of 120 GeV/c^2 where the analysis is most sensative. The current result increases sensitivity by $\sim$33% with 7.0 fb^{-1} of data and the addition of three improvements: (a) reducing jet backgrounds for regular central photons using a neural network (NN) discriminator, (b) including "plug" photons (1.2< $|\eta|$ <2.8), and (c) reconstructing central photons that convert into an electron-positron pair. The use of the latter two improvements allows for three new channels to be added: a central-plug (CP) category where two regular photons are found, one in the central region and one in the plug region; a central-central conversion category (CC conversion) where a regular central photon and a central conversion photon are identified; and a central-plug conversion category (CP conversion) where one regular plug photon and a central conversion photon are found. The first improvement, using a NN to identify central photons, most significantly enhances the CC channel where two central photons are selected, but additionally benefits the CP and CC conversions categories which also include central photons.

All cross sections are calculated by HIGLU and branching fractions are calculated by HDECAY [9]. These values are summarized in Table I.

M_h (GeV/c^2)	σ(*g fusion*) pb	$\sigma(W_{associated})$ pb	$\sigma(Z_{associated})$ pb	$\sigma(VBF)$ pb	$B(H \to \gamma\gamma)$
100	1.822	0.2919	0.1698	0.1001	0.0015
105	1.585	0.2484	0.1459	0.0923	0.0017
110	1.385	0.2120	0.1257	0.0851	0.0019
115	1.216	0.1745	0.1039	0.0786	0.0020
120	1.072	0.1501	0.0902	0.0727	0.0021
125	0.9493	0.1295	0.0785	0.0671	0.0022
130	0.8429	0.1120	0.0685	0.0621	0.0022
135	0.7508	0.0972	0.0600	0.0575	0.0021
140	0.6706	0.0846	0.0527	0.0532	0.0019
145	0.6006	0.0737	0.0463	0.0494	0.0017
150	0.5391	0.0644	0.0408	0.0458	0.0014

TABLE I: Production cross sections for SM Higgs production and branching fractions for SM Higgs decays.

II. THE CDF DETECTOR

The CDF detector is described in many available references [15, 16].

III. DATA SETS AND GLOBAL EVENT SELECTION

This analysis uses data from February 2004 and June 2010 comprising approximately 7.0 fb^{-1} of integrated luminosity. Signal Monte Carlo (MC) was generated using PYTHIA 6.2 [10] using CTEQ5 [11] parton distribution functions,

and the standard CDF underlying event tune [12]. Samples for masses between 100 – 150 GeV/c^2 in 5 GeV/c^2 intervals were developed and used.

The global event selection requires that the data was taken during good detector conditions, that the event vertex be within $|z_{vtx}| < 60$ cm, that the two photons have transverse energy E_T >15 GeV, and that their invariant mass be greater than 30 GeV/c^2. This selection is exactly the same as the published high-mass search for Randall-Sundrum gravitons decaying to the $\gamma\gamma$ final state [13] and therefore will not be discussed in detail here. The only difference for this result is that a different trigger is used, which is described below.

Recent diphoton analyses at CDF have used diphoton triggers [8, 13]. Photon conversions, however, are suppressed by these triggers due to a requirement that an electromagnetic (EM) cluster profile be consistent with that of an isolated single EM object. In order to increase acceptance for photon conversions, it was decided instead to use a high-p_T inclusive photon trigger which relaxes this requirement. This trigger additionally requires one cluster of electromagnetic energy to have $E_T > 25$ GeV, the EM cluster be loosly isolated, and that only a small fraction of the total E_T associated with the cluster be hadronic. It was found that this trigger in place of the diphoton triggers provides about the same acceptance in the regular photon channels, but greater acceptance in the conversion channels.

The inclusive photon trigger efficiency for our cuts in each channel was obtained using Higgs diphoton MC samples. For each photon in an event, simulated trigger variables were determined assuming trigger tower clustering and a $z_{vtx} = 0$ cm. If at least one photon in the event passed all trigger selection, then the trigger efficiency for each channel was obtained by taking the ratio of the events that pass all diphoton selection and the trigger to those that pass the diphoton selection.

The resulting efficiencies applied for each test mass and channel are plotted in Figure 1. The trigger efficiencies for the CC channel are about 100%, as they were for the diphoton trigger used in previous diphoton analyses. For the CP channel they range from about 96-100% from lower to higher masses, for the CC conversion channel they range from 98-99% and for the CP conversion channel they range from 90-97%. The statistical binomial errors seen in the figure are applied as systematic uncertainties. The uncertainty for the CC and CP channels are < 0.1% so are ignored. For the CC (CP) conversion channel the maximum uncertainty from the test masses is 0.2% (0.4%), which is applied as the systematic error.

IV. PHOTON IDENTIFICATION

A. Central Photon ID

In the 5.4 fb^{-1} result, central photons were selected using a standard set of cut-based photon selection at CDF [8]. A new method of selecting photons with $|\eta| < 1.05$ was recently developed that takes advantage of a neural network in order to better distinguish true prompt photons from jet backgrounds such as π^0 and η mesons. Since the electron signature is similar to that of photons except for a track, electrons are rejected using the standard set of track cuts that

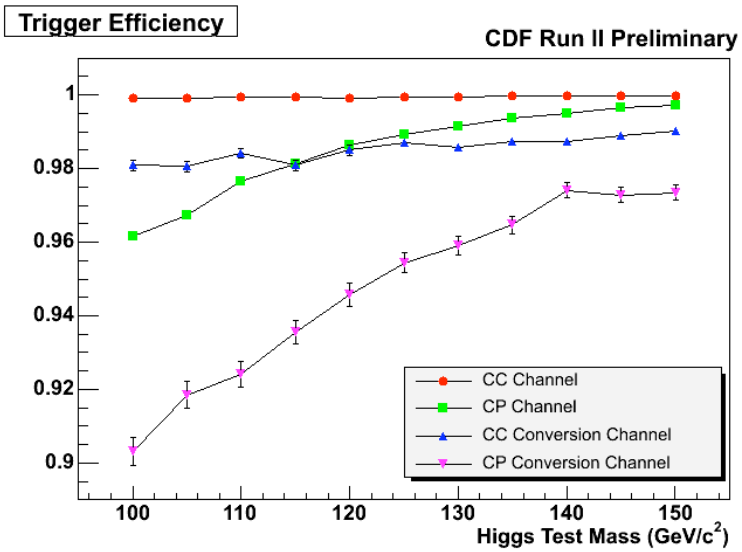

FIG. 1: Trigger efficiencies for each mass and channel are shown with statistical binomial errors.

have been used in the past. This also allows for the possibility of calculating a data-MC scale factor from $Z \to e^+e^-$ events, where the track cuts are modified to allow a single track.

The selection is given in three steps: (a) loose photon cuts are first applied in order to let the neural net be responsible for harder cases where a jet looks more closely like a photon, (b) standard tight tracking cuts are applied in order to reject electrons and some jets and lastly (c) a cut on the neural network output is applied. Loose cuts require the photons to be in the well instrumented region of the shower maximum detector (fiduciality) and allows for relaxed selection on isolation and the fraction of hadronic E_T. Tighter selection rejects events with significant clusters nearby and events with one or more tracks associated with the electromagnetic cluster that have significant transverse momentum. Finally, a cut on the NN output is applied, optimized for the SM $H \to \gamma\gamma$ analysis.

For the CC channel as an example, this selection provides a signal efficiency of 95.5% and background rejection of 81.3%, an improvement from standard cuts which gave 91.6% signal efficiency and 70.6% background rejection.

Efficiencies were calculated using $Z \to e^+e^-$ decays in both data and MC, as a function of the number of vertices in the event. Net efficiencies were obtained by folding the resulting values into the distribution of the number of vertices in the event for the diphoton data and Higgs MC simulation. A correction factor of 94.7% is derived for the ID efficiency of the simulation by comparing the ID efficiency from the detector simulation with that measured in the data.

Several sources of systematic uncertainty were considered. Photon ID efficiencies are studied using electrons from Z boson decays, however, there are small differences in the shower profiles of electrons and photons which may affect these studies. To account for this, a systematic of 1% was taken based on the difference between photon and electron ID efficiencies observed in the MC with detector simulation. For this comparison, $\gamma \to e^+e^-$ conversions were removed from the photon MC which are not in the Z MC. An uncertainty of 0.2% on the efficiency of removing these conversions is applied and is due to the uncertainty on material included in the simulation of the CDF detector. A single data-MC scale factor is applied to the full MC sample, however, the variations of this factor between data taking periods was included as a systematic of 1.5%. Finally, the uncertainties on the fits used to study ID efficiencies are propagated as an uncertainty of 0.2%.

B. Plug Photon ID

We include photons with $1.2 < |\eta| < 2.8$ using standard CDF photon ID including fiduciality, isolation, an insignificant fraction of hadronic E_T, and and transverse shower profiles consistent with a single photon. Scale factors are obtained using the same techniques as for central photons, resulting in a simulation correction factor of 90.7%. The same sources of systematic uncertainty on photon ID for central photons are applied to plug photons. Uncertainty from the difference between electron vs photon ID is taken to be 2.6%, from detector material to be 3.0%, from data taking periods to be 2.0%, and from data/MC fits to be 0.8%.

C. Central Conversion Photon ID

As photons pass through detector material, electromagnetic interactions with a nucleus can cause photons to convert into an electron-positron pair. Using photon MC truth information it was found that this occurs approximately 15% of the time in the central region of the detector, so for the CC channel about 26% of events are lost (where we ignore double conversion events) and about 15% of events are lost in the CP channel. Due to lower tracking efficiency in the plug region we only consider central conversion photons.

For the CC and CP conversion channels, events are first considered if a single regular photon is found either in the central or plug region using the identification described in previous sections (thus also rejecting events with a regular CC or CP diphoton pair). A base set of selection is then applied that searches for a primary central electron with a colinear, oppositely signed track nearby. The proximity of the two electron tracks is determined from their $r-\phi$ separation and $\Delta\cot\theta$, or separation in $\cot\theta = p_z/p_T$. "Trident" $e + (\gamma \to e^+e^-)$ events are rejected by finding cases where there are two tracks near the primary electron that pass this base selection — these are events where an electron radiates a photon via bremsstrahlung which then converts to an electron-positron pair.

A tighter set of selection is then applied to this base criteria. The tracks from both electrons are to point to a fiducial electromagnetic energy cluster (or clusters if in different calorimeter towers). Photons of a higher p_T range are are selected by requiring the secondary electron to have a $p_T > 1.0$ GeV/c and the reconstructed conversion photon have $p_T > 15$ GeV/c. In order to reject jet backgrounds, only a small fraction of hadronic E_T associated with the primary electron's cluster is allowed. Additionally, requirements are made on the conversion candidate's calorimeter isolation which is obtained from the primary electron's isolation energy with the secondary electron's p_T subtracted if it's track points to a different calorimeter phi tower. The shape describing the ratio of transverse energy to transverse

momentum (E/P) is peaked at one for for isolated photon conversions, but has a long tail for photon conversions from π^0 or $\eta \to \gamma\gamma$ decays due to the extra energy from the unconverted photon. Restrictions on this ratio then provide a further way to remove jet backgrounds. The conversion E_T is obtained from the primary electron's E_T with the secondary electron's p_T added if it is in a different calorimeter tower while the photon's reconstructed transverse momentum is obtained by adding the vector sum of the two tracks momenta at the radius of the conversion. A final requirement removes events with a small radius of conversion, primarily to reduce prompt electron-positron pairs from Dalitz decays of neutral pions $\pi^0 \to e^+e^-\gamma$.

In order to obtain an uncertainty on identifying the pair conversions, Z decays in both data and MC were again studied as with regular photons. However, after tagging one tight electron, rather than searching for another isolated electron a trident event was studied in order to probe the conversion from the radiated photon. Due to the lower energy range of the conversion photons of this method compared to those from $H \to \gamma\gamma$, it was chosen not to apply a data-MC scale factor to simulated events but instead to use the difference in the calculated scale factor from one to obtain an uncertainty on conversion ID. This was estimated by comparing the ratio of number of trident events selected to the number of regular $Z \to e^+e^-$ events selected in both the data and MC. This ratio was chosen in order to remove dependence on uncertainties from sources such as trigger efficiency, luminosity, and Z cross section. The result gives a 7% uncertainty which is applied as a systematic on conversion ID.

V. DETECTOR ACCEPTANCE

The detector acceptance was studied using PYTHIA Monte Carlo production events passed through a simulation for the CDF detector, CDFSIM, based on GEANT [17] and GFLASH [18]. The remaining events that additionally passed the same photon ID selection as the data, were then used to obtain an overall signal acceptance for each signal process and mass point. These values are given in Table II.

VI. SYSTEMATIC UNCERTAINTIES ON SIGNAL

Systematic uncertainties on signal MC are summarized in Table III and include uncertainties in the production cross section, the integrated luminosity, and on the acceptance and efficiency. A 6% uncertainty on the integrated luminosity considers uncertainty in $p\bar{p}$ inelastic cross section and acceptance of CDF's luminosity monitor. The theoretical uncertainties on the production cross sections used are 14% for gluon fusion, 7% for associative Higgs production with a W or Z, and 5% for vector boson fusion. All systematics on ID efficiency for photons were described in section IV.

The PDF uncertainty on event acceptance was calculated using the CTEQ61.M [19, 20] error sets and a standard event re-weighting technique [21, 22]. Initial and final state radiation (ISR and FSR) uncertainties were studied using MC samples with modified parton shower parameters. The energy scale systematic uncertainty of the central/plug electromagnetic calorimeters (CEM/PEM) was studied by checking the effect on the acceptance of varying the CEM/PEM scale by 1% to obtain 0.1% for central and 0.8% for plug.

The vertex systematic takes into account the efficiency of reconstructing vertices in an event. Since events are required to lie in the region of the detector consistent with $p\bar{p}$ interactions, the vertex systematic additionally takes into account the fraction of collisions that do not.

VII. BACKGROUND MODEL

The width of the $M_{\gamma\gamma}$ signal peak for each channel (shown in Figure 2) is on the order of a few GeV/c^2 and is only limited by detector resolution. This means that in general we are searching for a very narrow peak on a smooth background distribution. For regular photons, this smooth region of the data is composed of both SM diphoton events and events in which one or two jets fake a photon. For conversion photons, this region of the data is mostly composed of real conversions from jets and jets faking a conversion photon. Modeling of the background combinations is possible, but non-trivial, and is not necessary for dedicated searches for a narrow mass peak. Therefore, rather than model each background component directly, a null hypothesis is assumed — after visual confirmation that no significant peak exists in the data, a smooth curve is fit to the data. This fit excludes a 12 GeV/c^2 window around each mass point and is then interpolated into the signal region. The fit in the 12 GeV/c^2 signal region serves as the background model for predicting the expected sensitivity and for testing against the data for the signal hypotheses at the various mass points.

Production Process	M_H (GeV/c^2)	Signal Acceptances (%) CC	CP	CC Conv	CP Conv
ggH	100	12.0	15.8	2.7	1.8
	105	12.1	15.9	2.8	1.8
	110	12.2	16.2	2.7	1.8
	115	12.4	16.2	2.8	1.8
	120	12.5	16.3	2.9	1.9
	125	12.6	16.3	2.9	1.8
	130	12.7	16.3	2.9	1.8
	135	12.9	16.2	2.9	1.8
	140	13.0	16.3	2.9	1.8
	145	13.3	16.3	2.9	1.9
	150	13.3	16.2	3.0	1.8
VH	100	12.4	14.0	2.7	1.4
	105	12.4	14.2	2.7	1.6
	110	12.6	14.4	2.7	1.5
	115	12.7	14.6	2.7	1.5
	120	12.7	14.7	2.8	1.6
	125	12.9	14.7	2.8	1.6
	130	13.0	14.8	2.8	1.6
	135	13.0	14.9	2.8	1.6
	140	13.2	14.9	2.8	1.6
	145	13.2	15.0	2.8	1.6
	150	13.3	15.0	2.8	1.6
VBF	100	13.4	14.1	3.0	1.5
	105	13.5	14.5	3.0	1.6
	110	13.6	14.7	3.1	1.6
	115	13.8	14.8	3.1	1.6
	120	13.8	15.0	3.1	1.6
	125	13.8	15.1	3.1	1.6
	130	14.0	15.2	3.2	1.7
	135	14.0	15.2	3.1	1.7
	140	14.2	15.3	3.1	1.7
	145	14.2	15.2	3.1	1.7
	150	14.4	15.2	3.2	1.6

TABLE II: Signal acceptance for each signal process, mass point, and channel.

One modification to this method is made for the CP channels that are contaminated by a large contribution of Z $\rightarrow e^+e^-$ backgrounds which is visible as a peak in the data. The Z background could be modeled by MC and added then to the smooth portion, but we can also more simply further our current method by adding an appropriate function to describe the peak made by the Z boson. It was found that a Breit-Wigner function well describes this region of the $M_{\gamma\gamma}$ distribution for the CP channels, so it was added to the smooth function used to fit to the rest of the data.

An example fit for each channel, obtained from a mass window around 120 GeV/c^2, is shown in Figures 3 – 4, along with the corresponding residual plot of (data – fit)/(stat error). The stability of the fits in the 12 GeV/c^2 signal region used for setting limits was studied by fluctuating the parameter values of the fit and and then taking the average of the smallest and largest integral differences from that of the standard function. In general, these values reflect the statistics in the respective mass distributions as higher statistics constrains the amount by which the fit will fluctuate as parameter values are varied. The results were used to obtain a background rate uncertainty for each channel and mass with about 3.5%, 1.1%, 7.5%, and 3.5% applied to the CC, CP, CC conversion, and CP conversion channels respectively. Cross checks on these values were done by either replacing or modifying the fit function. From these studies, variations of the test background yields in the signal regions as compared to that of the standard were consistent with uncertainties already obtained.

CDF Run II Preliminary $\int \mathcal{L} = 7.0$ fb^{-1}

	Systematic Errors on Signal (%)			
	CC	CP	CC Conv	CP Conv
Luminosity	6	6	6	6
$\sigma_{ggH}/\sigma_{VH}/\sigma_{VBF}$	14/ 7/ 5	14/ 7/ 5	14/ 7/ 5	14/ 7/ 5
PDF	2	2	2	2
ISR	3	4	2	5
FSR	3	4	2	5
Energy Scale	0.2	0.8	0.1	0.8
Trigger Efficiency	–	–	0.1	0.4
Z Vertex	0.2	0.2	0.2	0.2
Conversion ID	–	–	7	7
Material Uncertainty	0.4	3.0	0.2	3.0
Photon/Electron ID	1.0	2.8	1.0	2.6
Run Dependence	3.0	2.5	1.5	2.0
Data/MC fits	0.4	0.8	1.5	2.0

TABLE III: Summary of systematic errors applied to signal.

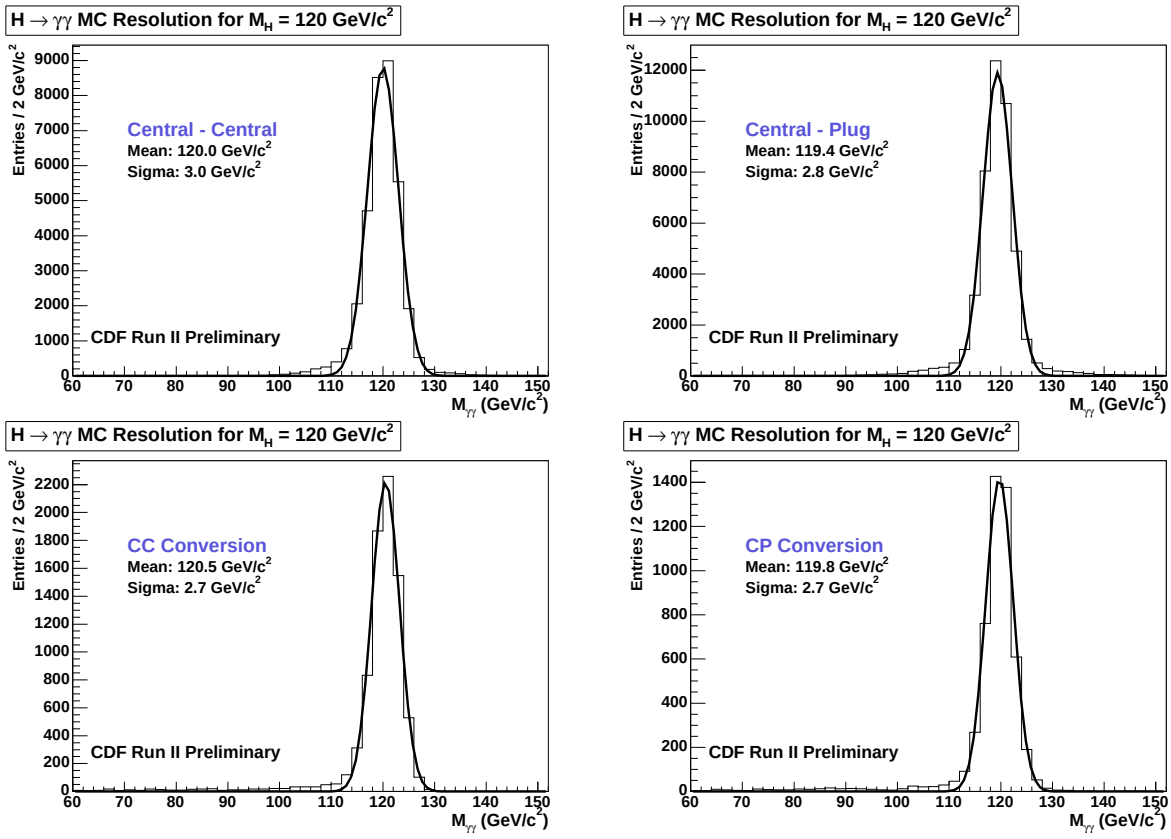

FIG. 2: Invariant mass distribution for each channel for a theoretical Higgs mass of $M_h = 120$ GeV/c^2, showing a Gaussian width of $\sigma = 3$ GeV/c^2 or less.

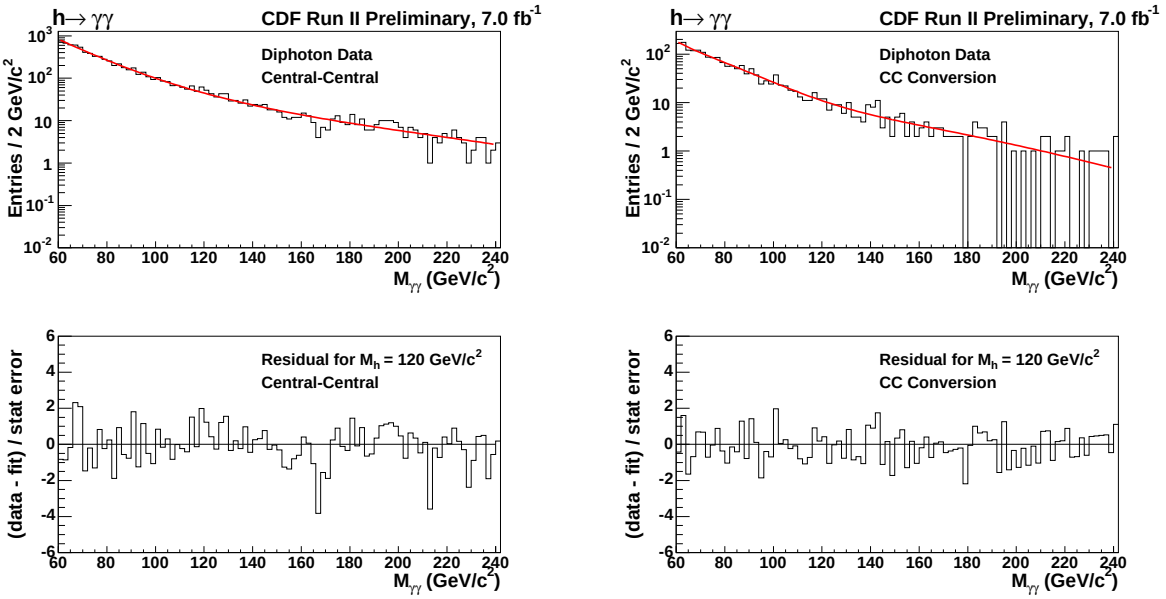

FIG. 3: Smooth fits to the signal region in the data for CC channels with the SM Higgs event selection. The example fit shown was obtained by first excluding a 12 GeV/c^2 window around a signal mass of $M_h = 120$ GeV/c^2 and then interpolating into this region. The fit in the signal region will serve as the null hypothesis background model. The data-fit residual is also shown.

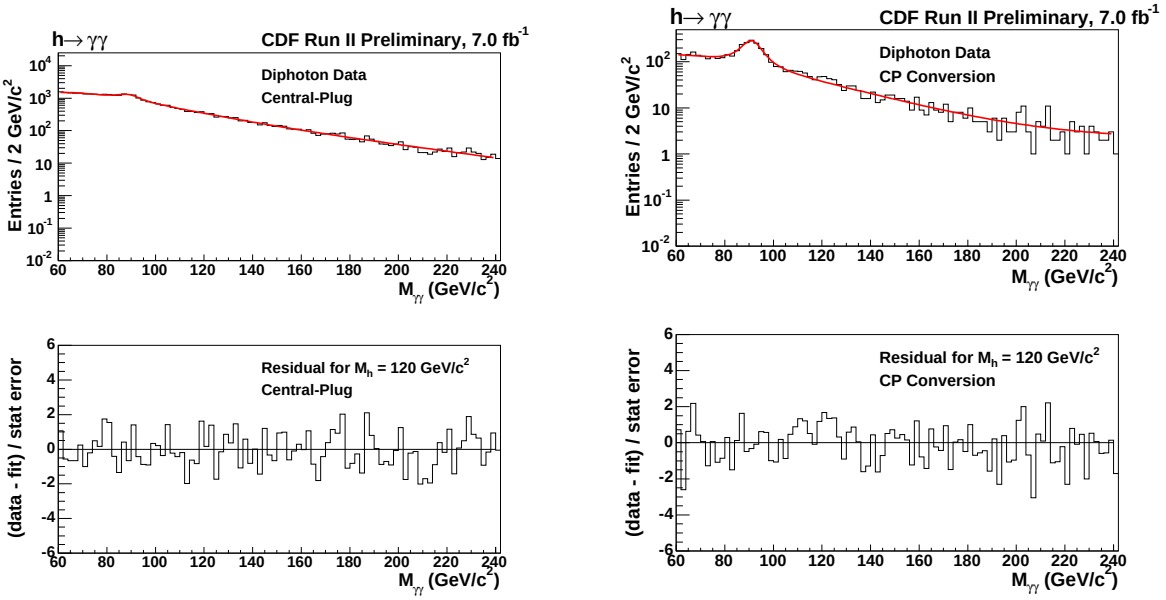

FIG. 4: A smooth fit combined with a fit function to model the Z $\rightarrow e + e-$ contribution for the CP channels. These example plots show fits to the signal region in the data with the SM Higgs event selection. The example fit shown was obtained by first excluding a 12 GeV/c^2 window around a signal mass of $M_h = 120$ GeV/c^2 and then interpolating into this region. The fit in the signal region will serve as the null hypothesis background model. The data-fit residual is also shown.

VIII. RESULTS

Upper limits are set on production cross sections times branching ratio. The theoretical production cross section and branching fraction were given in Table I and detector acceptance for each mass point is in Table II. These values, as well as the invariant mass distributions for the signal and background model, are used to set limits on $H \to \gamma\gamma$ production. Only the 12 GeV/c^2 signal region of the $M_{\gamma\gamma}$ distributions is used in obtaining these limits.

A binned-likelihood method is applied using Poisson fluctuations of the $M_{\gamma\gamma}$ bin contents in order to set limits on sensitivity to the $H \to \gamma\gamma$ signal hypothesis. From the combination of all channels, the 95% confidence level limits on cross section multiplied by branching fraction relative to the SM prediction are summarized in Table IV and shown in Figure 5. The observed limit at 120 GeV/c^2 is outside of two sigma band, however taking trial factor into account reduces this significance below two sigma.

Limits for each channel alone at 120 GeV/c^2 can be found in Table V. The invariant mass distribution of the two photons for each channel with data, background, and signal shapes for an example Higgs test mass of 120 GeV/c^2 is also shown in Figure 6.

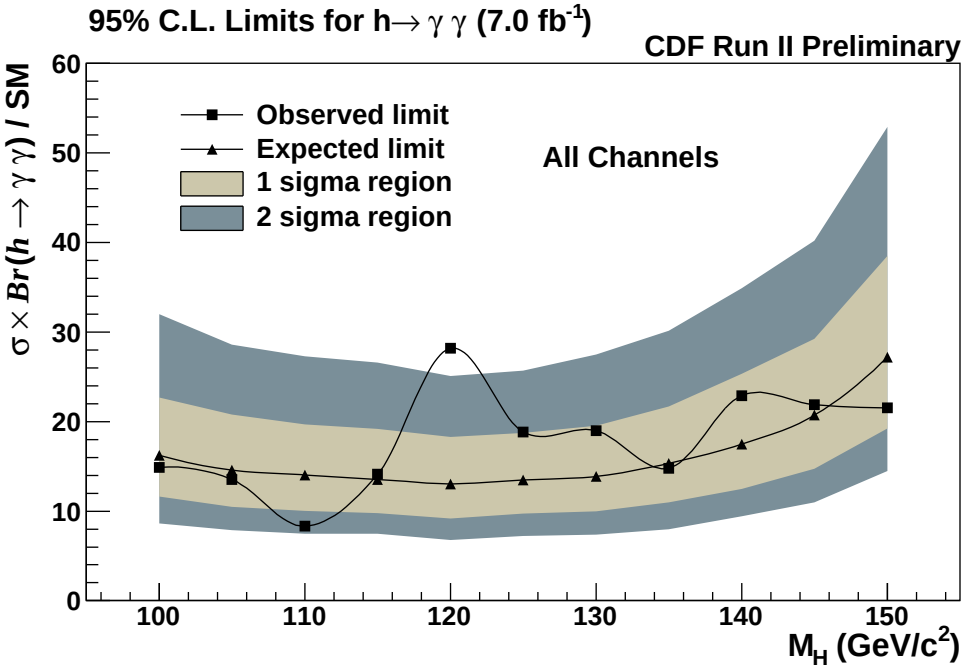

FIG. 5: Cross section times branching fraction limits relative to the SM as a function of Higgs mass.

CDF Run II Preliminary $\int \mathcal{L} = 7.0$ fb^{-1}

M_H	95% C.L. Limit/σ(SM)×$B(h \to \gamma\gamma)$					
(GeV/c^2)	-2σ	-1σ	Median Exp	+1σ	+2σ	Observed
100	8.7	11.6	16.2	22.7	32.0	14.9
105	7.9	10.5	14.6	20.8	28.6	13.5
110	7.5	10.1	14.0	19.7	27.3	8.3
115	7.5	9.8	13.5	19.2	26.6	14.1
120	6.8	9.2	13.0	18.3	25.1	28.2
125	7.2	9.7	13.5	18.7	25.7	18.8
130	7.4	10.0	13.9	19.6	27.5	19.0
135	8.0	11.0	15.3	21.7	30.1	14.8
140	9.4	12.5	17.5	25.4	34.9	22.9
145	11.0	14.7	20.7	29.3	40.2	21.9
150	14.5	19.2	27.2	38.5	52.9	21.5

TABLE IV: 95% upper confidence level limits on cross sections times branching ratio relative to SM prediction for all channels combined.

CDF Run II Preliminary						$\int \mathcal{L} = 7.0$ fb^{-1}
Channel	95% C.L. Limit/σ(SM)$\times B(h \to \gamma\gamma)$					
Alone	-2σ	-1σ	Median Exp	+1σ	+2σ	Observed
CC	8.4	11.6	16.2	23.14	32.0	32.0
CP	18.4	24.7	35.3	50.3	67.8	50.4
CC Conv	17.2	23.8	32.9	46.8	66.7	35.5
CP Conv	60.5	81.9	115.5	166.0	229.5	243.7

TABLE V: 95% upper confidence level limits on cross sections times branching ratio relative to SM prediction for each channel alone at a test mass of 120 GeV/c^2.

IX. CONCLUSIONS

An analysis was discussed which searched for $H \to \gamma\gamma$ in 7.0 fb^{-1} of CDF data using central photons from an improved ID, forward photons, and central conversion photons. No significant excess over the background was observed, so we presented 95% C.L. upper limits on the production cross sections times branching fraction relative to the SM expectation. For Higgs masses between 100 and 150 GeV the expected limits range from 13.0 to 27.2 and observed limits range from 8.2 to 28.2. This is an approximate 33% improvement from the previous result using 5.4 fb^{-1}.

Acknowledgments

We thank the Fermilab staff and the technical staffs of the participating institutions for their vital contributions. This work was supported by the U.S. Department of Energy and National Science Foundation; the Italian Istituto Nazionale di Fisica Nucleare; the Ministry of Education, Culture, Sports, Science and Technology of Japan; the Natural Sciences and Engineering Research Council of Canada; the National Science Council of the Republic of China; the Swiss National Science Foundation; the A.P. Sloan Foundation; the Bundesministerium fuer Bildung und Forschung, Germany; the Korean Science and Engineering Foundation and the Korean Research Foundation; the Particle Physics and Astronomy Research Council and the Royal Society, UK; the Russian Foundation for Basic Research; the Comision Interministerial de Ciencia y Tecnologia, Spain; and in part by the European Community's Human Potential Programme under contract HPRN-CT-20002, and the Academy of Finland.

[1] S. Mrenna and J. D. Wells, Phys. Rev. **D63**, 015006 (2001), hep-ph/0001226.
[2] G. L. Landsberg and K. T. Matchev, Phys. Rev. **D62**, 035004 (2000), hep-ex/0001007.
[3] L. Authors (LEP Higgs Working Group) (2001), hep-ex/0107035.
[4] A. A. Affolder et al. (CDF), Phys. Rev. **D64**, 092002 (2001), hep-ex/0105066.
[5] V. Abazov et al. (D0) (2008), arXiv:0803.1514 [hep-ex].
[6] T. Aaltonen et al. (CDF), Phys. Rev. Lett. **103**, 061803 (2009), 0905.0413.
[7] V. Abazov et al. (D0), Phys. Rev. Lett. **102**, 231801 (2009).
[8] C. collaboration (CDF) (2010), CDF note 10065.
[9] M. Spira (1998), hep-ph/9810289.
[10] T. Sjostrand et al., Comput. Phys. Commun. **135**, 238 (2001), hep-ph/0010017.
[11] H. L. Lai et al. (CTEQ), Eur. Phys. J. **C12**, 375 (2000), hep-ph/9903282.
[12] R. Field and R. C. Group (CDF) (2005), hep-ph/0510198.
[13] T. Aaltonen et al. (CDF) (2007), arXiv:0707.2294 [hep-ex].
[14] S. Wynne, R. Culbertson, and T. Berry (CDF) (2006), CDF note 8359.
[15] F. Abe et al. (CDF), Nucl. Instr. Meth. **A271**, 387 (1988).
[16] P. T. Lukens (CDF IIb) (2003), FERMILAB-TM-2198.
[17] R. Brun, F. Bruyant, M. Maire, A. C. McPherson, and P. Zanarini (1987), CERN-DD/EE/84-1.
[18] G. Grindhammer, M. Rudowicz, and S. Peters, Nucl. Instrum. Meth. **A290**, 469 (1990).
[19] D. Stump et al., JHEP **10**, 046 (2003), hep-ph/0303013.
[20] J. Pumplin et al., Phys. Rev. **D65**, 014013 (2002), hep-ph/0101032.
[21] P. M. Nadolsky and Z. Sullivan, eConf **C010630**, P510 (2001), hep-ph/0110378.
[22] D. Bourilkov, R. C. Group, and M. R. Whalley (2006), hep-ph/0605240.

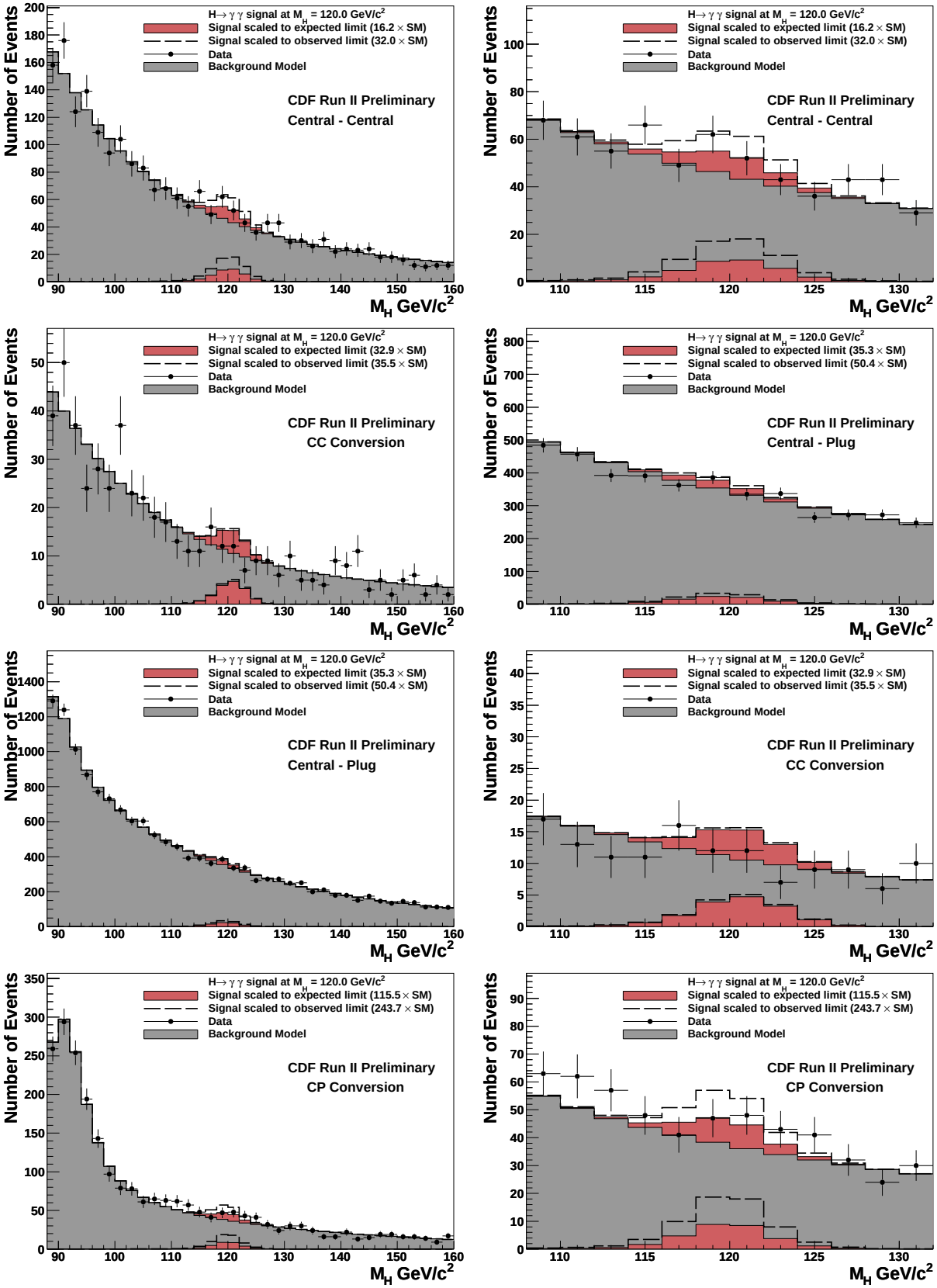

FIG. 6: Invariant mass distribution over whole mass range and zoomed in, with an example theoretical Higgs mass at 120 GeV/c^2, scaled to the expected and observed limits obtained from the respective channel alone.